Depth-dependent cerebral hemodynamic responses following Direct Cortical Electrical Stimulation (DCES) revealed by *in vivo* dual-optical imaging techniques

Seungduk Lee,[1] Dalkwon Koh,[2] Areum Jo,[3] Hae Young Lim,[3] Young-Jin Jung,[4] Choong-Ki Kim,[2] Youngwook Seo,[2] Chang-Hwan Im,[4] Beop-Min Kim, [2,*] and Minah Suh [3,*]

[1] *Department of Biomicrosystem Engineering, Korea University, Jeongneung 3-dong, Seongbuk-ku, Seoul, 136-703, South Korea*

[2] *Department of Biomedical Engineering, Korea University, Jeongneung 3-dong, Seongbuk-ku, Seoul, 136-703, South Korea*

[3] *Department of Life Science, Sungkyunkwan University, Cheonchoen-dong, Jangan-gu, Suwon, 440-746, South Korea*

[4] *Department of Biomedical Engineering, Hanyang University, Wangsimni-ro, Seongdong-gu, Seoul, 133-791, South Korea*

[*]*minahsuh@skku.edu*

Abstract: We studied depth-dependent cerebral hemodynamic responses of rat brain following direct cortical electrical stimulation (DCES) *in vivo* with optical recording of intrinsic signal (ORIS) and near-infrared spectroscopy (NIRS). ORIS is used to visualize the immediate hemodynamic changes in cortical areas following the stimulation, whereas NIRS measures the hemodynamic changes originating from subcortical areas. We found strong hemodynamic changes in relation to DCES both in ORIS and NIRS data. In particular, the signals originating from cortical areas exhibited a tri-phasic response, whereas those originating from subcortical regions exhibited multi-phasic responses. In addition, NIRS signals from two different sets of source-detector separation were compared and analyzed to investigate the causality of perfusion, which demonstrated downstream propagation, indicating that the upper brain region reacted faster than the deep region.

©2012 Optical Society of America

OCIS codes: (170.0170) Medical optics and biotechnology; (170.2655) Functional monitoring and imaging; (170.6510) Spectroscopy, tissue diagnostics.

References and links

1. A. Grinvald, E. Lieke, R. D. Frostig, C. D. Gilbert, and T. N. Wiesel, "Functional architecture of cortex revealed by optical imaging of intrinsic signals," Nature **324**(6095), 361–364 (1986).
2. A. Zepeda, C. Arias, and F. Sengpiel, "Optical imaging of intrinsic signals: recent developments in the methodology and its applications," J. Neurosci. Methods **136**(1), 1–21 (2004).
3. B. R. Chen, M. B. Bouchard, A. F. McCaslin, S. A. Burgess, and E. M. Hillman, "High-speed vascular dynamics of the hemodynamic response," Neuroimage **54**(2), 1021–1030 (2011).
4. A. Devor, A. K. Dunn, M. L. Andermann, I. Ulbert, D. A. Boas, and A. M. Dale, "Coupling of total hemoglobin concentration, oxygenation, and neural activity in rat somatosensory cortex," Neuron **39**(2), 353–359 (2003).
5. A. Devor, I. Ulbert, A. K. Dunn, S. N. Narayanan, S. R. Jones, M. L. Andermann, D. A. Boas, and A. M. Dale, "Coupling of the cortical hemodynamic response to cortical and thalamic neuronal activity," Proc. Natl. Acad. Sci. U.S.A. **102**(10), 3822–3827 (2005).
6. R. D. Frostig, E. E. Lieke, D. Y. Ts'o, and A. Grinvald, "Cortical functional architecture and local coupling between neuronal activity and the microcirculation revealed by in vivo high-resolution optical imaging of intrinsic signals," Proc. Natl. Acad. Sci. U.S.A. **87**(16), 6082–6086 (1990).
7. H. Gurden, N. Uchida, and Z. F. Mainen, "Sensory-evoked intrinsic optical signals in the olfactory bulb are coupled to glutamate release and uptake," Neuron **52**(2), 335–345 (2006).
8. Y. B. Sirotin, E. M. Hillman, C. Bordier, and A. Das, "Spatiotemporal precision and hemodynamic mechanism of optical point spreads in alert primates," Proc. Natl. Acad. Sci. U.S.A. **106**(43), 18390–18395 (2009).

9. J. Sepulcre, J. C. Masdeu, M. A. Pastor, J. Goñi, C. Barbosa, B. Bejarano, and P. Villoslada, "Brain pathways of verbal working memory: a lesion-function correlation study," Neuroimage **47**(2), 773–778 (2009).
10. R. Sitaram, H. H. Zhang, C. T. Guan, M. Thulasidas, Y. Hoshi, A. Ishikawa, K. Shimizu, and N. Birbaumer, "Temporal classification of multichannel near-infrared spectroscopy signals of motor imagery for developing a brain-computer interface," Neuroimage **34**(4), 1416–1427 (2007).
11. C. H. Im, Y. J. Jung, S. Lee, D. Koh, D. W. Kim, and B. M. Kim, "Estimation of directional coupling between cortical areas using Near-Infrared Spectroscopy (NIRS)," Opt. Express **18**(6), 5730–5739 (2010).
12. S. Lee, M. Lee, D. Koh, B. M. Kim, and J. H. Choi, "Cerebral hemodynamic responses to seizure in the mouse brain: simultaneous near-infrared spectroscopy-electroencephalography study," J. Biomed. Opt. **15**(3), 037010 (2010).
13. N. Roche-Labarbe, B. Zaaimi, M. Mahmoudzadeh, V. Osharina, A. Wallois, A. Nehlig, R. Grebe, and F. Wallois, "NIRS-measured oxy- and deoxyhemoglobin changes associated with EEG spike-and-wave discharges in a genetic model of absence epilepsy: the GAERS," Epilepsia **51**(8), 1374–1384 (2010).
14. J. W. Scannell, G. A. P. C. Burns, C. C. Hilgetag, M. A. O'Neil, and M. P. Young, "The connectional organization of the cortico-thalamic system of the cat," Cereb. Cortex **9**(3), 277–299 (1999).
15. H. J. Alitto and W. M. Usrey, "Corticothalamic feedback and sensory processing," Curr. Opin. Neurobiol. **13**(4), 440–445 (2003).
16. H. Blumenfeld and D. A. McCormick, "Corticothalamic inputs control the pattern of activity generated in thalamocortical networks," J. Neurosci. **20**(13), 5153–5162 (2000).
17. J. A. Buckwalter, J. Parvizi, R. J. Morecraft, and G. W. van Hoesen, "Thalamic projections to the posteromedial cortex in the macaque," J. Comp. Neurol. **507**(5), 1709–1733 (2008).
18. P. Tian, I. C. Teng, L. D. May, R. Kurz, K. Lu, M. Scadeng, E. M. Hillman, A. J. De Crespigny, H. E. D'Arceuil, J. B. Mandeville, J. J. Marota, B. R. Rosen, T. T. Liu, D. A. Boas, R. B. Buxton, A. M. Dale, and A. Devor, "Cortical depth-specific microvascular dilation underlies laminar differences in blood oxygenation level-dependent functional MRI signal," Proc. Natl. Acad. Sci. U.S.A. **107**(34), 15246–15251 (2010).
19. F. Zhao, P. Wang, K. Hendrich, K. Ugurbil, and S. G. Kim, "Cortical layer-dependent BOLD and CBV responses measured by spin-echo and gradient-echo fMRI: insights into hemodynamic regulation," Neuroimage **30**(4), 1149–1160 (2006).
20. L. Seungduk, J. L. Hyun, I. Changkyun, S. Hyung-Cheul, K. Dalkwon, and K. Beop-Min, "Simultaneous Measurement of Hemodynamic and Neuronal Activities Using Near-infrared Spectroscopy and Single-unit Recording," J Korean Phys Soc **58**(6), 1697–1702 (2011).
21. S. Lee, D. Koh, K. Kwon, H. J. Lee, Y. Lang, H. C. Shin, and B. M. Kim, "Hemodynamic responses of rat brain measured by near-infrared spectroscopy during various whisker stimulations," J Opt Soc Korea **13**(1), 166–170 (2009).
22. M. S. Patterson, S. Andersson-Engels, B. C. Wilson, and E. K. Osei, "Absorption spectroscopy in tissue-simulating materials: a theoretical and experimental study of photon paths," Appl. Opt. **34**(1), 22–30 (1995).
23. G. Paxinos and C. Watson, *The Rat Brain in Stereotaxic Coordinates,* 6th ed. (Academic Press/Elsevier, Amsterdam Boston, 2007).
24. B. Champagne, M. Eizenman, and S. Pasupathy, "Exact maximum likelihood time delay estimation for short observation intervals," IEEE Trans. Signal Process. **39**(6), 1245–1257 (1991).
25. C. Knapp and G. Carter, "The generalized correlation method for estimation of time delay," IEEE Trans. Acoust Speech **24**(4), 320–327 (1976).
26. A. Piersol, "Time delay estimation using phase data," IEEE Trans. Acoust Speech **29**(3), 471–477 (1981).
27. M. Azaria and D. Hertz, "Time delay estimation by generalized cross correlation methods," IEEE Trans. Acoust Speech **32**(2), 280–285 (1984).
28. J. Benesty, J. Chen, and Y. Huang, "Time-delay estimation via linear interpolation and cross correlation," IEEE Trans. Speech Audi P **12**(5), 509–519 (2004).
29. M. Kamiński, M. Z. Ding, W. A. Truccolo, and S. L. Bressler, "Evaluating causal relations in neural systems: granger causality, directed transfer function and statistical assessment of significance," Biol. Cybern. **85**(2), 145–157 (2001).
30. J. Theiler, S. Eubank, A. Longtin, B. Galdrikian, and J. D. Farmer, "Testing for nonlinearity in time-series - the method of surrogate data," Physica D **58**(1-4), 77–94 (1992).
31. T. Schreiber and A. Schmitz, "Surrogate time series," Physica D **142**(3-4), 346–382 (2000).
32. J. Neter, W. Wasserman, and M. H. Kutner, *Applied Linear Regression Models,* 2nd ed. (Irwin, Homewood, Ill., 1989), pp. xv, 667.
33. D. Liebetanz, F. Fregni, K. K. Monte-Silva, M. B. Oliveira, A. Amâncio-dos-Santos, M. A. Nitsche, and R. C. Guedes, "After-effects of transcranial direct current stimulation (tDCS) on cortical spreading depression," Neurosci. Lett. **398**(1-2), 85–90 (2006).
34. F. Fregni, P. S. Boggio, M. A. Nitsche, M. A. Marcolin, S. P. Rigonatti, and A. Pascual-Leone, "Treatment of major depression with transcranial direct current stimulation," Bipolar Disord. **8**(2), 203–204 (2006).
35. F. Hummel, P. Celnik, P. Giraux, A. Floel, W. H. Wu, C. Gerloff, and L. G. Cohen, "Effects of non-invasive cortical stimulation on skilled motor function in chronic stroke," Brain **128**(3), 490–499 (2005).
36. X. Zheng, D. C. Alsop, and G. Schlaug, "Regional modulation of BOLD MRI responses to human sensorimotor activation by transcranial direct current stimulation," Neuroimage **45**, 196–201 (2011).

37. J. Baudewig, M. A. Nitsche, W. Paulus, and J. Frahm, "Regional modulation of BOLD MRI responses to human sensorimotor activation by transcranial direct current stimulation," Magn. Reson. Med. **45**(2), 196–201 (2001).
38. T. Kamida, S. Kong, N. Eshima, T. Abe, M. Fujiki, and H. Kobayashi, "Transcranial direct current stimulation decreases convulsions and spatial memory deficits following pilocarpine-induced status epilepticus in immature rats," Behav. Brain Res. **217**(1), 99–103 (2011).
39. D. P. Purpura and J. G. McMurtry, "Intracellular Activities and Evoked Potential Changes during Polarization of Motor Cortex," J. Neurophysiol. **28**, 166–185 (1965).
40. N. Prakash, J. D. Biag, S. A. Sheth, S. Mitsuyama, J. Theriot, C. Ramachandra, and A. W. Toga, "Temporal profiles and 2-dimensional oxy-, deoxy-, and total-hemoglobin somatosensory maps in rat versus mouse cortex," Neuroimage **37**(Suppl 1), S27–S36 (2007).
41. M. Wolf, U. Wolf, V. Toronov, A. Michalos, L. A. Paunescu, J. H. Choi, and E. Gratton, "Different time evolution of oxyhemoglobin and deoxyhemoglobin concentration changes in the visual and motor cortices during functional stimulation: a near-infrared spectroscopy study," Neuroimage **16**(3), 704–712 (2002).
42. I. Vanzetta and A. Grinvald, "Evidence and lack of evidence for the initial dip in the anesthetized rat: implications for human functional brain imaging," Neuroimage **13**(6), 959–967 (2001).
43. R. B. Buxton, "The elusive initial dip," Neuroimage **13**(6), 953–958 (2001).
44. J. C. Siero, N. Petridou, H. Hoogduin, P. R. Luijten, and N. F. Ramsey, "Cortical depth-dependent temporal dynamics of the BOLD response in the human brain," J. Cereb. Blood Flow Metab. **31**(10), 1999–2008 (2011).

1. Introduction

Since its first introduction [1], optical imaging techniques have been used widely to monitor real-time changes in blood perfusion and oxygenation *in vivo* [2]. Optical recording of intrinsic signal (ORIS) is capable of measuring changes in light absorption associated with neuronal activity without adding contrast agent. ORIS has been applied to various neuroscience studies due to its high spatiotemporal resolution [3–8]. However, ORIS mainly provides hemodynamic information only from the superficial layer of the cortex because of its low penetration depth. Near-infrared spectroscopy (NIRS), another optical imaging technique, noninvasively measures hemodynamic responses in deeper brain regions by sacrificing the spatial resolution compared to ORIS. Because of the high temporal resolution, NIRS has been widely applied in various neuroscientific studies including cognition [9], brain-computer interface (BCI) [10], functional brain connectivity [11], and neurological disease [12, 13].

Neural connectivity between different brain regions is extremely important for determining brain function [14]. The reciprocal relationship between the cerebral cortex and thalamus has been well understood as projective organizations and a feedback system [15–17]. Depth-dependent hemodynamic responses to sensory stimulation have been reported within the cortical layer of human [18] and cat [19]. When the visual stimulus was applied, the hemodynamic responses of deeper gray matter are significantly faster than the responses of the pial structures [18], suggesting the temporal dynamics of hemodynamic responses can be highly specific to the cortical depth. However, these studies were limited to cortical areas which did not include the deeper subcortical brain area. Therefore, in this study, we investigated whether the cerebral hemodynamic responses to direct cortical electrical stimulation (DCES) is depth dependent by ORIS and NIRS recoding. Our main interest was the differences and similarities of hemodynamic signals measured in both cortical and subcortical areas. The DCES strategy was employed to achieve an enhanced signal-to-noise ratio (SNR) of the hemodynamic signal. The NIRS signals obtained from two different sets of source-detector separations, which spans different depth subcortical regions, were considered.

2. Materials and Methods

2.1 Animal preparation

Seven adult rats (Sprague–Dawley, 8-10 weeks) were used in this experiment. All animal preparation and experimental procedures followed institutional guidelines of the Animal Care and Use Committee of Sungkyunkwan University. Animals were anesthetized with isoflurane (Hana Pharm., Seoul, South Korea) and oxygen gas. The level of anesthesia was closely monitored during the experiment based on the toe-pinch reflex test, breathing pattern, and blood pressure. During the surgical procedure, animals were placed on a stereotaxic frame,

and temperature was maintained using a heating pad. After cutting the midline skin of the head, the skull near the somatosensory cortex was exposed and thinned using a drill. A small burr hole was made in the thinned skull area, and the dura was carefully removed. A tungsten electrode (Plastics One, Roanoke, V.A., U.S.A.) connected to an electrical stimulator (Master 8, AMPI, Jerusalem, Israel) was placed in the burr hole of the somatosensory cortex (anterior-posterior: −1.5 mm from bregma, lateral: ±5.0 mm from midline). The location of the thinned skull is shown in Fig. 1
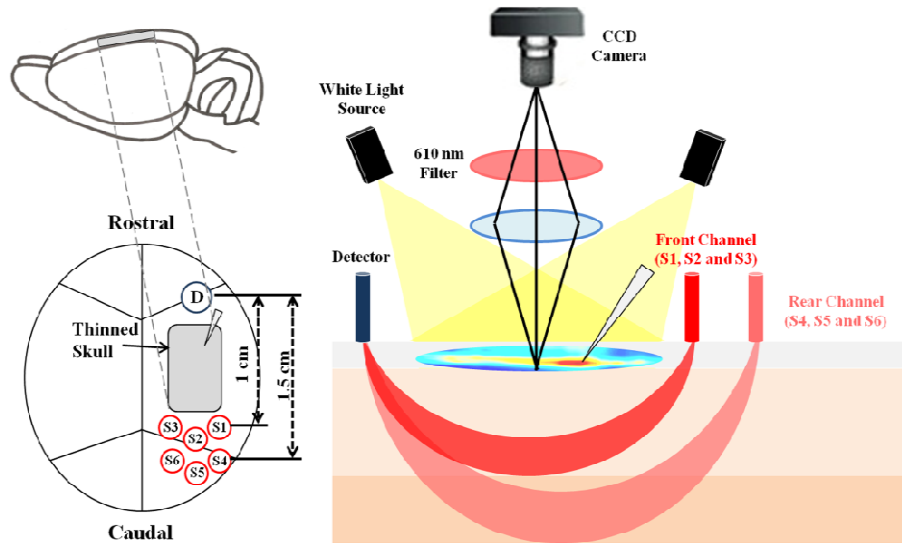

Fig. 1. Experimental scheme for simultaneous optical recording of intrinsic signal (ORIS) and near-infrared spectroscopy (NIRS)

2.2 ORIS Imaging and Data Analysis

An Optical Imager 3001 system (Optical-Imaging, Inc., Jerusalem, Israel) was used to perform ORIS imaging. A halogen lamp illuminated the target brain, and reflected light was filtered using a 610 nm band pass filter. The recorded image is highly correlated with the deoxyhemoglobin concentration. As deoxyhemoglobin increases, the reflected signal becomes darker due to the high absorption coefficient. The image plane of a CCD camera (Adimec-1000m, Adimec, Eindhoven, Netherlands) was located 500 μm below the cortical surface. Image acquisition was performed at 1000 frames for 10 minutes (1.67 Hz). The event (stimulation)-related changes in light reflectance amplitude were acquired by dividing each frame with the average images obtained for 30 seconds prior to DCES, as described below. Changes in light reflectance were calculated as $-\Delta R/R$ (%) using the Matlab program (Mathworks, Natick, M.A., U.S.A.).

2.3 NIRS Setup

A custom-manufactured continuous-wave NIRS system [20] was used to measure the cerebral hemodynamic responses to DCES in the rat brain. Six pairs of optical fibers with a 400 μm core diameter (FT-400EMT, Thorlabs, Newton, N.J., U.S.A.) were arranged as shown in Fig. 1. Each pair, composed of two wavelengths (690 and 830 nm), was held in place using custom-made manipulating arms [21]. Light penetration depth is proportional to approximately one-half or one-third of the source-detector distance in highly scattering media [22] such as the brain. Two different source-detector distances of 1 cm (front channels) and 1.5 cm (rear channels) were used to evaluate hemodynamic axial variation. Front channels are sufficient to cover deep layers of the somatosensory cortex and hippocampus and rear

channels are sufficient to cover globus pallidus and ventral posterior nucleus of thalamus [23]. The NIRS signal sampling rate was about 30 Hz.

2.4 Direct Cortical Electrical Stimulation (DCES) and Imaging Trials

Monophasic trains of electrical pulses were delivered at a frequency of 3.3 Hz for 10 seconds (Fig. 2) via a stimulator (Master 8, AMPI) and an isolator (ISU, AMPI). The current amplitude of the stimulation was 1 mA. The stimulation parameters were recorded on a computer via the Spike2 (CED, Cambridge, U.K.) software for clarification. Imaging was performed in a quiet and dark room. Each imaging trial lasted 10 minutes, after the stimulation session and inter-trial interval, which were 30 minutes. NIRS and ORIS were recorded sequentially to reduce optical interference in the detectors (Fig. 2).
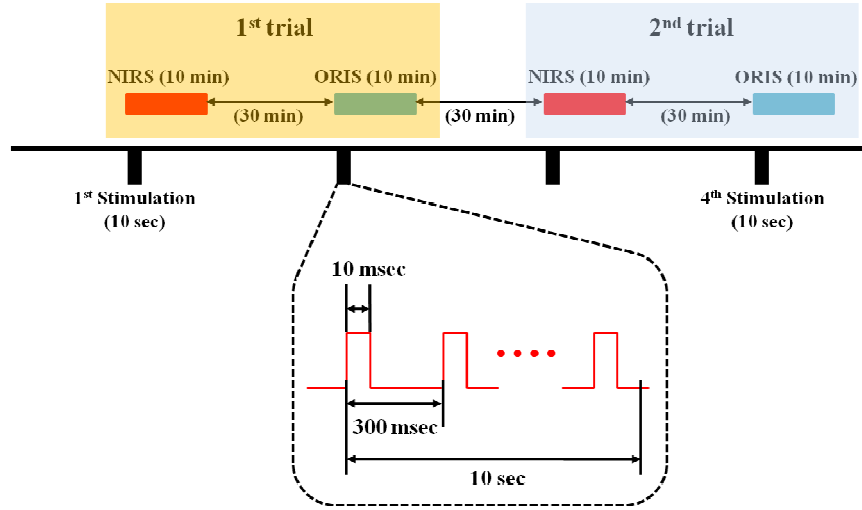

Fig. 2. Stimulation paradigm and imaging with ORIS and NIRS. Monophasic trains with pulse widths of 10 msec were delivered at a frequency of 3.3 Hz for 10 seconds. NIRS and ORIS were alternatively applied every 30 minutes.

2.5 NIRS Data Analysis

The 690 and the 830 nm signals were converted to oxy- (ΔHbO_2) and deoxyhemoglobin (ΔHbr) concentrations using the modified Beer–Lambert law as described in Eq. (1).

$$\Delta OD^{\lambda} = -\ln \frac{I_{Final}}{I_{Initial}} = (\varepsilon_{HbO_2}^{\lambda} \Delta[HbO_2] + \varepsilon_{Hbr}^{\lambda} \Delta[Hbr])B^{\lambda}L, \qquad (1)$$

where I_{Final} is the light intensity transmitted through biological tissue to a detector, $I_{Initial}$ is the initial light intensity. ε is the extinction coefficient, B indicates the differential pathlength factor, L is the source-detector distance, and λ is wavelength (690 and 830 nm). Using the calculated ΔOD^{λ}, we extracted ΔHbO_2 and ΔHbr using the following equations:

$$\Delta[HbO_2] = \frac{\varepsilon_{Hbr}^{\lambda_1} \dfrac{\Delta OD^{\lambda_2}}{B^{\lambda_2}} - \varepsilon_{Hbr}^{\lambda_2} \dfrac{\Delta OD^{\lambda_1}}{B^{\lambda_1}}}{(\varepsilon_{Hbr}^{\lambda_1} \varepsilon_{HbO_2}^{\lambda_2} - \varepsilon_{Hbr}^{\lambda_2} \varepsilon_{HbO_2}^{\lambda_1})L}, \qquad (2)$$

and

$$\Delta[Hbr] = \frac{\varepsilon_{HbO_2}^{\lambda_2} \dfrac{\Delta OD^{\lambda_1}}{B^{\lambda_1}} - \varepsilon_{HbO_2}^{\lambda_1} \dfrac{\Delta OD^{\lambda_2}}{B^{\lambda_2}}}{(\varepsilon_{Hbr}^{\lambda_1}\varepsilon_{HbO_2}^{\lambda_2} - \varepsilon_{Hbr}^{\lambda_2}\varepsilon_{HbO_2}^{\lambda_1})L}. \tag{3}$$

A symmetric high-pass filter (tenth-order zero phase Butterworth with f_c = 0.01 Hz) was applied to remove the low frequency drift noise. We analyzed the ΔHbr signal only to compare the NIRS signal to the ORIS signal, as ORIS images only reflect the deoxyhemoglobin concentration changes.

2.6 Causality Analysis

We adopted a time delay estimation method to evaluate the causal relationship between the front (S1, S2 and S3) and rear (S4, S5 and S6) NIRS channels, which is one of the most traditional ways to estimate causal interactions between two time series [24–26]. To date, various time-delay estimation procedures have been proposed and implemented, including cross-correlation functions, mutual entropy estimation, phase slope, maximum likelihood estimation, and others [24–26]. Among them, the cross-correlation function was employed in this study, because it could provide robust and accurate time delay estimates between two signals with very similar low-frequency temporal patterns and statistically independent noises [27, 28]. Before the causality analysis, we applied a low pass filter with a cutoff frequency of 1 Hz to the raw signals

Considering that two time series, $X(t)$ and $Y(t)$, have independent noise components, $n_X(t)$ and $n_Y(t)$, respectively, the cross-correlation function between the two time series can be represented by:

$$R_{XY}(\tau) = E[X(t)Y(t-\tau)] \tag{4}$$

where "E" is the expected value operator, and τ is the time lag. Then, the time delay d_{XY} is defined as the time lag τ when the cross-correlation function $R_{XY}(\tau)$ has the maximum value. The sign of the time delay, d_{XY}, also suggests a causal relationship between the two signals X and Y. When $d_{XY} > 0$, $X(t)$ causes $Y(t)$; otherwise ($d_{XY} < 0$), $Y(t)$ causes $X(t)$. It is obvious that the above process is valid only when the maximum correlation between $X(t)$ and $Y(t - d_{XY})$ is significantly high (see the below paragraph for the statistical significance test).

We employed a statistical evaluation process called a surrogate test to test whether the estimated causal interaction was statistically meaningful. The surrogate test has been widely used to determine the significance of the causal interaction between brain signals [29, 30]. Generally, the correlation between two time signals is destroyed when the phases of the two time signals are randomly shuffled. In the present study, we generated large size surrogate data sets (1000 data) for each pair of detectors by randomly and independently rearranging time series phases acquired from each position of the rat brain [31]. Then, the empirical distributions of the surrogate data cross-correlation values were estimated to determine the significance level, for which we selected the top 5% values from each distribution ($p < 0.05$).

2.7 Complexity Evaluation of NIRS and ORIS Signal Patterns

We calculated a coefficient of determination (R^2), using third polynomial fitting, to evaluate the complexity of the NIRS and ORIS signal patterns. The coefficient of determination was obtained as described in Eq. (5) [32].

$$R^2 = \frac{SSR}{SSTO} = 1 - \frac{SSE}{SSTO}. \tag{5}$$

where $SSR = \sum(\hat{Y}_i - \bar{Y}_i)^2$ is the regression sum of squares, Y_i and $\hat{Y}_i$ are the observed and predicted values in the data set, respectively, and $\bar{Y}_i$ is the mean of the observed data.

$SSE = \sum (Y_i - \hat{Y}_i)^2$ is the error sum of squares, also called residual sum of squares, and $SSTO = \sum (Y_i - \bar{Y}_i)^2$ is total sum of squares. As $0 \leq SSE \leq SSTO$, it follows that: $0 \leq R^2 \leq 1$.

3. Results

The ORIS and NIRS data consecutively obtained during DCES were analyzed and compared. Because the sampling rates of the ORIS and the NIRS data were different, the NIRS data were down-sampled using a 30 point moving average, and the ORIS and NIRS data were normalized with the maximum value. The time courses of the front channels (S1, S2 and S3) were averaged as well as the rear NIRS data.
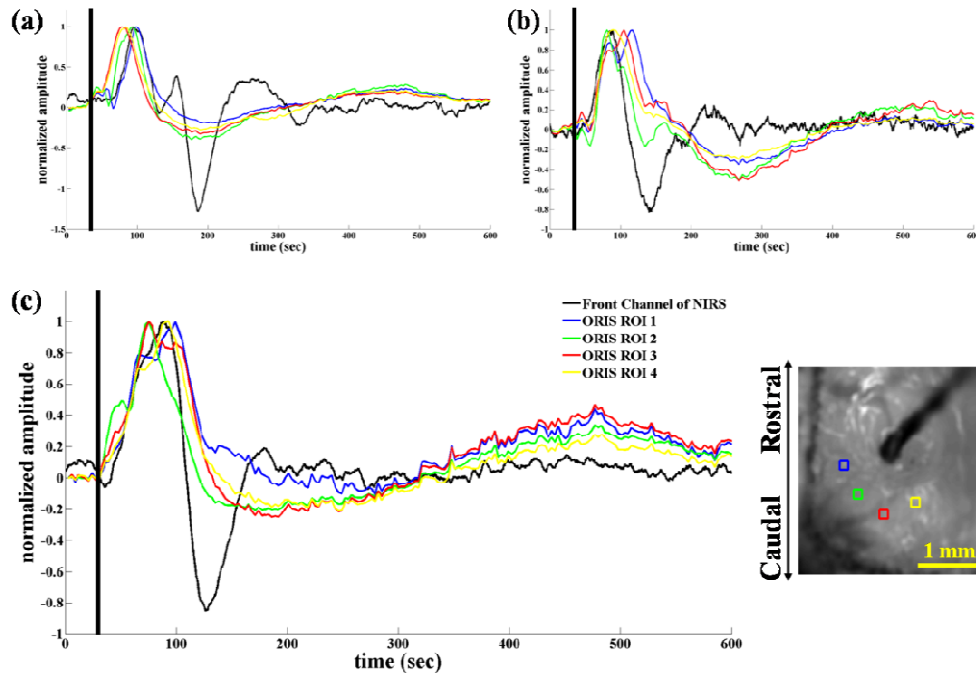

Fig. 3. Time courses of the hemodynamic responses and the ORIS and NIRS to DCES in three subjects (a) rat #2, (b) rat #7 and (c) rat #4. The hemodynamic responses were normalized to the maximum peak value. Black color indicates changes in the NIRS deoxyhemoglobin (△Hbr) signal averaged by the front channels (channels 1, 2, and 3). Blue, green, red and yellow color represents ORIS regions of interest (ROIs) 1, 2, 3 and 4, respectively, as shown in the exposed cortical surface image.

Figure 3 shows the normalized amplitude changes in ΔHbr concentrations for three subjects during the first trial of the imaging session (10 minutes). Four regions of interest (ROIs) were selected around the stimulation electrode from the ORIS images, but avoiding large blood vessels. The average values of the front channels of the NIRS data are also illustrated in Fig. 3. Apparently, the ΔHbr concentration fluctuated for longer than 10 minutes after DCES in both the ORIS and NIRS data. In general, both cortical (ORIS) and deep subcortical (NIRS) brain hemodynamic signals changed significantly immediately after the electrical stimulation. However, the long-term responses in ΔHbr were notably different between the NIRS and ORIS signals. The ΔHbr concentration changes in the cortical brain (ORIS) showed a typical tri-phasic response pattern, whereas the ΔHbr from the deeper subcortical brain region (NIRS) demonstrated multi-phasic signal changes. The pattern of hemodynamic responses obtained with ORIS of the whole cortical area is illustrated in Fig. 6. The strip-image (long rectangle) was obtained by adding all pixels of the x-axis values at each

y-axis value. The red color indicates an increase in ΔHbr. The 10-second long stimulation induced a long-term hemodynamic effect in the cortical area, resulting in a tri-phasic response, as described earlier.

We calculated a coefficient of determination for both the NIRS and ORIS signals to quantitatively evaluate the differences in the signal patterns after applying third polynomial fitting for the first 5 minutes. The third polynomial fitting was chosen because the cortical hemodynamic responses patterns were mostly a triphasic in our experiment. If the coefficient of determination is large, then the third polynomial fitting well represents the hemodynamic signal pattern. In contrast, a low coefficient of determination implies that the signal changes were not close to the triphasic response pattern. Overall, the coefficient of determination for the NIRS signal (mean ± SD) was lower than that of the ORIS signal (mean ± SD). The values are summarized in Table 1.

Table 1. Coefficient of determination using third polynomial fitting for all subjects

	Rat 1	Rat 2	Rat 3	Rat 4	Rat 5	Rat 6	Rat 7	Average
1st ORIS (ROI 1)	0.39	0.79	0.80	0.69	0.69	0.64	0.67	**0.67±0.14**
2nd ORIS (ROI 1)	0.43	0.35	0.57	0.75	0.64	0.63	0.50	**0.55±0.14**
1st ORIS (ROI 2)	0.19	0.69	0.70	0.69	0.78	0.70	0.48	**0.60±0.20**
2nd ORIS (ROI 2)	0.21	0.51	0.27	0.62	0.70	0.60	0.71	**0.52±0.20**
1st NIRS (Front Channel)	0.16	0.09	0.03	0.15	0.15	0.45	0.01	**0.15±0.15**
2nd NIRS (Front Channel)	0.28	0.25	0.07	0.11	0.30	0.25	0.01	**0.18±0.12**
1st NIRS (Rear Channel)	0.24	0.30	0.08	0.14	0.30	0.50	0.03	**0.23±0.16**
2nd NIRS (Rear Channel)	0.33	0.39	0.10	0.13	0.19	0.26	0.03	**0.20±0.13**

More specifically, Fig. 4 shows a typical example of the time courses for the ΔHbr changes in the ORIS and NIRS signals during the first 170 seconds following stimulation. The first and second trials of a single rat imaging session are illustrated in Fig. 4(a) and 4(b), respectively. The two ORIS's ROIs were selected at near and far areas from the stimulating electrode. The NIRS channels were averaged for front (S1, S2, and S3) and rear channels (S4, S5 and S6). We expected to observe a temporal separation between the NIRS and ORIS data or between the front NIRS and rear NIRS data. However, the time to reach the first maximum was indistinguishable between any set of signal. The NIRS signals from the front and rear channels seemed to be separated in time slightly, even if it was difficult to statistically quantify the difference. These observations were consistent for all seven rats.
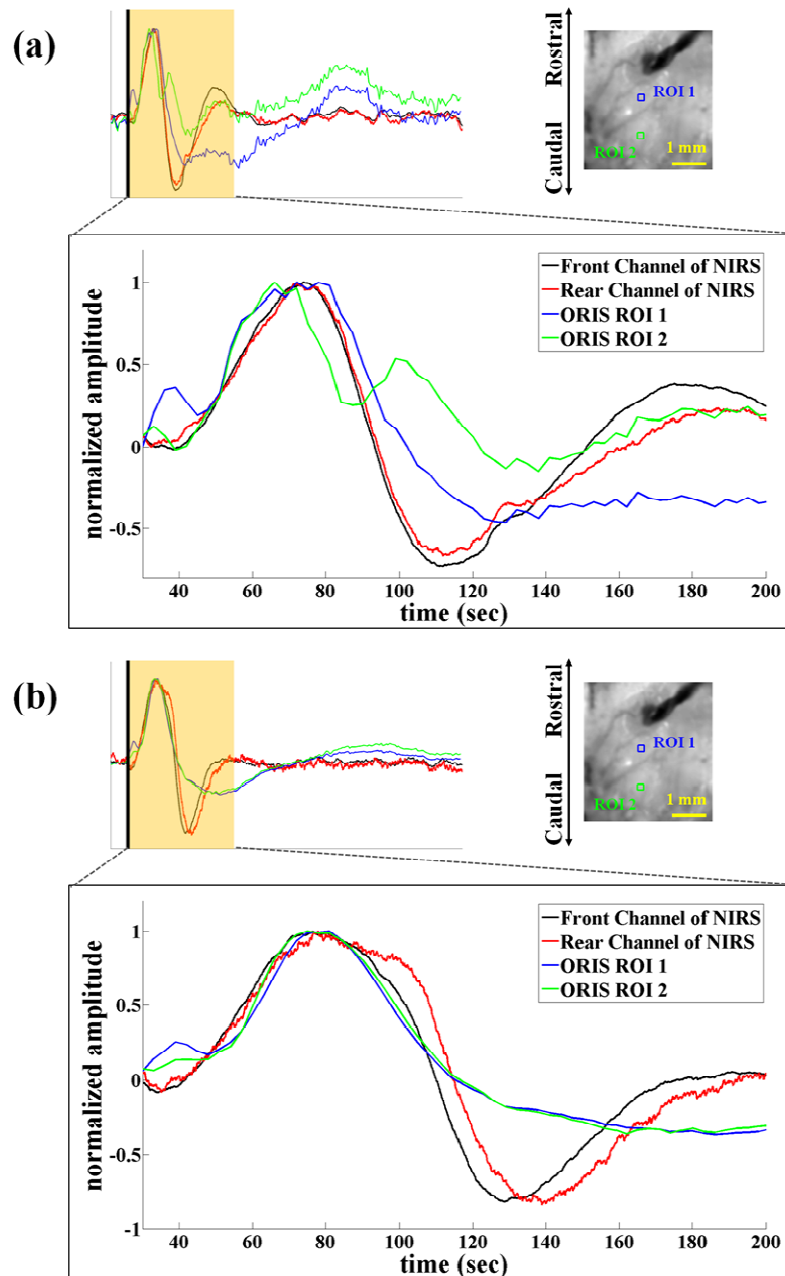
Fig. 4. Hemodynamic responses of ORIS and NIRS to DCES for two trials of an imaging session (a) first and (b) second trial during 170 seconds. A thick vertical black line in yellow area represents stimulation.

Therefore, the temporal difference between front and rear NIRS channels was further quantified using the causality analysis described earlier. The time delays between each pair of front and rear channels (S1↔S4, S2↔S5 and S3↔S6) were evaluated. Figure 5 illustrates the causal interaction between the front and rear channels of the NIRS signal. The arrows represent the directions of information flow. Statistically meaningless interactions are not depicted in the figure. The possible number of pairs for the front and rear channels was 42

(three pairs for each rat × seven rats × two events). Significant relationships between front and rear channels were demonstrated for approximately 92.9% (39 of 42) of the causality analyses. In particular, 79.5% (31 of 42) had a signal flow direction from the front to the rear channel, suggesting signal flow from the upper brain area to the deeper brain area. In particular, the channel 3 and channel 6 pair of all animals exhibited significant hemodynamic signal flow from the upper brain area to the deeper brain area. The average time delay between front and rear channels with statistically significant interaction was 5.84 seconds, corresponding to 175 time sampling points, which is large enough not to be significantly influenced by the background noise.
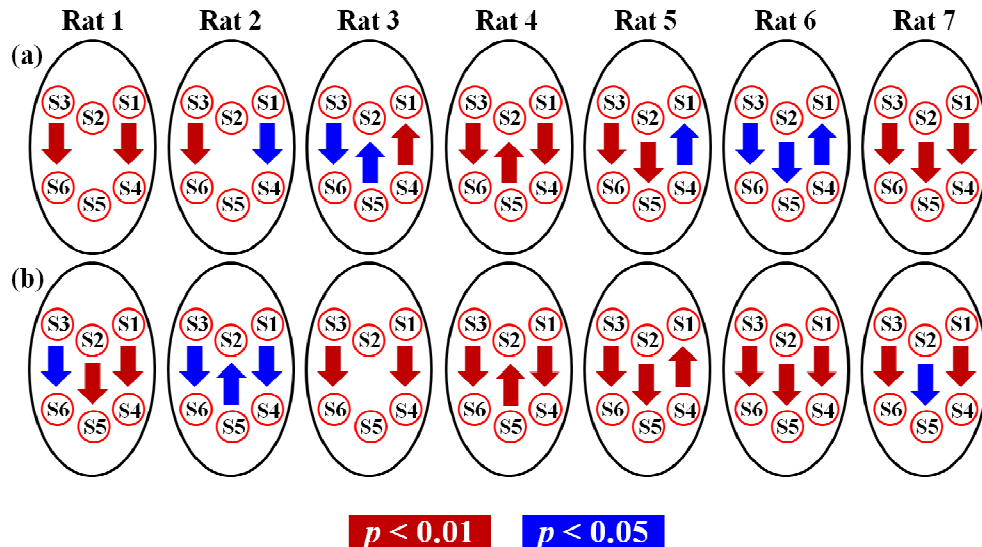

Fig. 5. Causal interaction between the front and rear NIRS channels signals for two trials (a) first and (b) second trial. Red arrows indicate a significant relationship with p<0.01 and blue arrows indicate a significant relationship with p<0.05. The arrow direction represents the signal flow direction.

4. Discussion

Neural connectivity is an important factor for the proper modulation of brain functions, including cognition and sensory-motor transformation. The cortex is a heavily interconnected brain area in both the horizontal and vertical directions and cortico-thalamic connection play very important role in shaping brain function. Recently, the cortical depth-dependent hemodynamic signal changes have been reported by using functional magnetic resonance imaging (fMRI) [18, 19]. The hemodynamic signals of deeper cortical gray matter reacted faster than the superficial area of the cortex in relation to sensory stimulus [18, 19]. But, these studies were limited to the cortical area. High spatial-resolution ORIS has also been widely used for studying cortical hemodynamics [1, 3–6, 8]. However, it is not appropriate for measuring hemodynamic responses in the deep subcortical brain area, as it measures the light reflected off of the surface of the cortex. In contrast, NIRS is a useful imaging technique with high temporal-resolution for dynamically measuring hemodynamics in deep brain areas, including subcortical reagion. In our NIRS setup, the distance between the source and detector was approximately 1–1.5 cm, which was adequate to measure hemodynamic responses from the deep subcortical brain area [22] such as the CA1 of hippocampus, globus pallidus and ventral posterior nucleus of thalamus regions in rat brain. Therefore, we combined the ORIS and NIRS techniques to effectively investigate depth-dependent variations in both the cortical and subcortical hemodynamic responses.
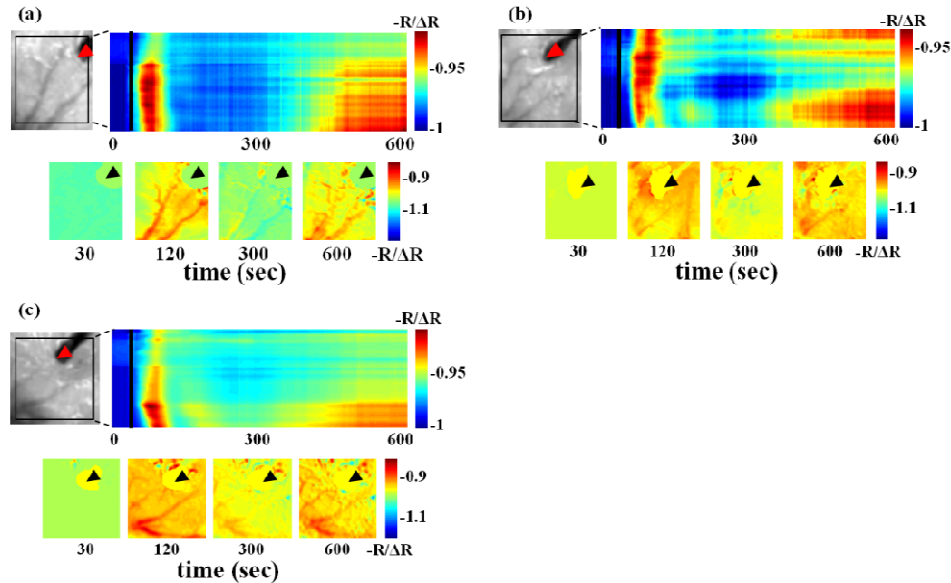
Fig. 6. The patterns of ORIS data following DCES. Examples from three different animals (a, b, & c) are presented. In each panel, the upper left image illustrates the imaged cortical area. The long rectangle is a strip-image of ORIS, which was obtained by adding all pixels of the x-axis values at each y-axis value. In the strip-image, a thick black line indicates the 10-second long direct electrical stimulation. In each panel, the bottom four images represent ORIS obtained at 30, 120, 300, and 600 seconds, respectively, during each trial. The black arrow head indicates the location of stimulating electrode. The red color indicates an increase in ΔHbr. A clear tri-phasic response was observed in all three examples.

We choose DCES method as our input protocol, because DCES induces large-scale and long-lasting changes in neuronal activities [33] following alterations of cortical excitability [34, 35]. DCES causes changes in cerebral blood flow [36], hemoglobin oxygenation state [37] and modulated *N*-methyl-D-aspartate (NMDA) receptor activity [38] in the cortical region. In our study, long lasting changes in deoxyhemoglobin concentrations in both the cortical and subcortical brain areas (Fig. 3) were observed. This result was consistent with previous experiments [33, 39]. Interestingly, the pattern of hemodynamic responses was different between cortical and subcortical brain areas. The ORIS ROI was selected by excluding large blood vessels to reduce vascular compartment dynamics [3]. In the cortical brain area, the deoxyhemoglobin concentration immediately increased after DCES due to a dramatic increase in oxygen consumption followed by a subsequent decrease in deoxyhemoglobin because of the oversupply of blood. Over the time course of 600 seconds, a secondary increase in deoxyhemoglobin was observed from the cortical brain area, exhibiting a tri-phasic response pattern [40]. However, the deoxyhemoglobin concentration in the deep subcortical brain area showed a multi-phasic response pattern. The third polynomial fitting analysis supported this result. This observation reflected the different depth-dependent hemodynamic responses between the deep subcortical brain and cortical area in response to DCES, causing explosive metabolic demand, as described in the one compartment model [41]. The different hemodynamic responses between ORIS and NIRS are due to their different source dependency, i.e. brain depth-dependency. The ORIS mainly reflects hemodynamic responses from the cortical area, whereas NIRS measures the hemodynamic responses in deep brain regions beyond the cortex.

We also investigated the short-term hemodynamic changes and found that the deoxyhemoglobin concentration in the cortical area initially increased (Fig. 4 and Fig. 6). This increased deoxyhemoglobin response could be associated with an initial dip, a mismatch of

hemodynamic due to sudden and large neuronal activation [42, 43], in the overall hemodynamic changes in the brain in response to DCES.

By causality analysis, we demonstrated that the front and rear channel NIRS signals were significantly correlated during DCES in the majority of our experimental cases. The analysis indicated that the NIRS signal tended to flow from the upper brain area to the deep subcortical brain area following direct stimulation onto the cortical tissue. In particular, the pair between the front and rear channel near the midline had the highest correlation, suggesting the upper brain region reacted faster than deep subcortical brain region [44].

We were unable to collect ORIS and NIRS data simultaneously, which was the major limitation of this study. The light used for ORIS data acquisition often saturated the NIRS detector, so they had to be used in turn. Even if multiple ORIS and NIRS measurements were obtained from a single subject, the hemodynamic responses were rather consistent across different trials. We closely monitored vital signs to ensure less inter-trial variability. In future studies, we plan to conduct simultaneous ORIS and the NIRS measurements by replacing the white light and filter combination with a 530 nm LED, which can be selectively filtered out on the NIRS detector side.

In conclusion, we successfully demonstrated the similarities and differences of depth-dependent cerebral hemodynamic responses. A sequential imaging of ORIS and NIRS provided a powerful technique to study the depth dependent hemodynamic signals of rat brain. The causality analyses strongly support that the spread of hemodynamic signals due to DCES mainly originated from the upper brain region to deep brain area. In other words, the cortical area reacted faster than the subcortical brain area to the direct electrical stimulation onto the cortical surface.